

We are IntechOpen, the world's leading publisher of Open Access books Built by scientists, for scientists

6,900

Open access books available

186,000

International authors and editors

200M

Downloads

Our authors are among the

154

Countries delivered to

TOP 1%

most cited scientists

12.2%

Contributors from top 500 universities



WEB OF SCIENCE™

Selection of our books indexed in the Book Citation Index
in Web of Science™ Core Collection (BKCI)

Interested in publishing with us?
Contact book.department@intechopen.com

Numbers displayed above are based on latest data collected.
For more information visit www.intechopen.com



Desalination by Membrane Distillation

*Mustakeem Mustakeem, Sofiane Soukane,
Muhammad Saqib Nawaz and Noredine Ghaffour*

Abstract

At present, around 25% of water desalination processes are based on distillation. Similar to classical distillation, membrane distillation is a phase-change process in which a hydrophobic membrane separates two phases. Membrane distillation is considered an emerging player in the desalination, food processing and water treatment market. Due to its high salt rejection, less fouling propensity, operating at moderate temperature and pressure, membrane distillation is considered as a future sustainable desalination technology. The distillation process is quite well known in desalination. However, membrane distillation emerged a few decades ago, and a thorough understanding is needed to adapt this technique in the near future. This review chapter introduces the classical distillation and membrane distillation as an emerging technology in the desalination arena. Heat and mass transfer and thermodynamics in membrane distillation, characteristics of the performance metrics of membrane distillation are also described. Finally, the performance evaluation of MD is presented. The possibility of using low-grade heat in membrane distillation allows it to integrate directly to solar energy and industrial waste heat.

Keywords: membrane distillation, desalination, vapor flux, vapor transport, evaporation

1. Introduction

Distillation is a thermal process in which a component separates out from a multi-component mixture by a phase-change process. When a membrane is put in between the feed and condensing solution, the feed can be vaporized and condensed at the membrane interface (thickness $\approx 200 \mu\text{m}$). **Figure 1** shows a schematic of a single-stage distillation and membrane distillation setup. The membrane distillation (MD) process combines the use of conventional distillation and membranes processes. It is a hybrid technology that uses the advantages of membrane separation and thermal distillation processes. In MD, the separation process employs a porous hydrophobic membrane between feed and permeate, allowing only solvent vapor to pass through, retaining the liquid/solid phase. Although the membrane provides a mass transfer resistance to the vapors, its employment allows water to condense within a minimal distance. This gives an advantage in creating a large partial pressure gradient across the membrane.

In a typical MD setup, the trans-membrane temperature difference (temperature difference between two sides of the membrane) creates the vapor pressure

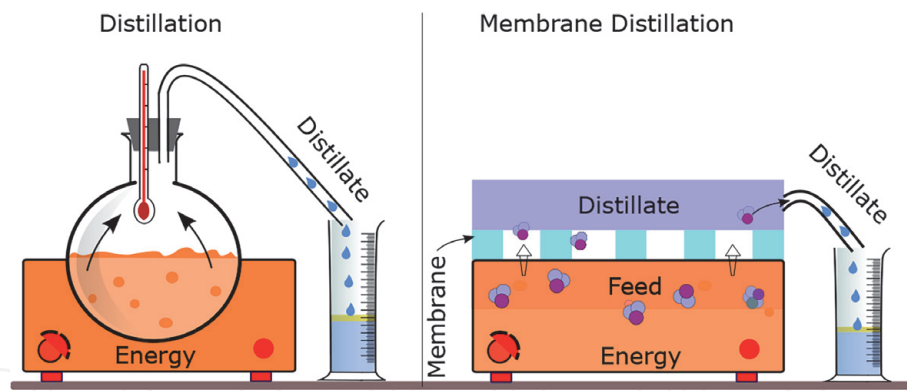


Figure 1.

A schematic of a typical single stage distillation system and the membrane distillation system. In MD, the vapors generate at the feed-membrane interface, and move to the permeate side and membrane allows only vapors to pass through.

difference, which drives mass transport [1–5]. The vapor is generated at the feed side and moves through the membrane pores to condense/get collected at the permeate side of the membrane. The salts, due to their non-volatile nature, remain in the feed solution.

MD has advantages over conventional desalination techniques. These include [6]:

- Low feed temperature in the range 50–90°C.
- Low fouling propensity.
- Capable to treat high saline water.
- High product water quality.
- Good compromise between specific enthalpy and efficiency.

Based on the distillate collection methods, MD can be classified into four broad configurations: (1) air gap membrane distillation (AGMD); (2) sweeping gas membrane distillation (SGMD); (3) vacuum membrane distillation (VMD); and (4) direct contact membrane distillation (DCMD) [7]. In all configurations, the feed solution remains in direct contact with one side of the membrane, while on the other side, distillate collection differs based on the type of the variant.

1. *Air gap membrane distillation:* In AGMD, the permeate side has an air gap followed by a condensing plate. A typical AGMD set up is shown in **Figure 2 (A)**. The vapor transfers from the hot feed to the air gap and eventually condenses at the cooling plate. The cooling plate can be cooled with multiple ways such as liquid cooled, air cooled, evaporative cooled; and gives the flexibility to use any coolant liquid as it does not mix with the condensate. AGMD is the most practical configuration in water production. However, due to high mass transfer resistance at permeate side, the flux is less as compared with other configurations. The air gap reduces the conduction heat loss from feed to permeate [8–10].
2. *Sweeping gas membrane distillation:* The SGMD uses a stream of gas to strip off the vapors from the permeate channel, after which they are either condensed externally or discarded as waste. **Figure 2(B)** shows a typical SGMD set up. SGMD shows less conduction heat loss than DCMD due to less conductivity of

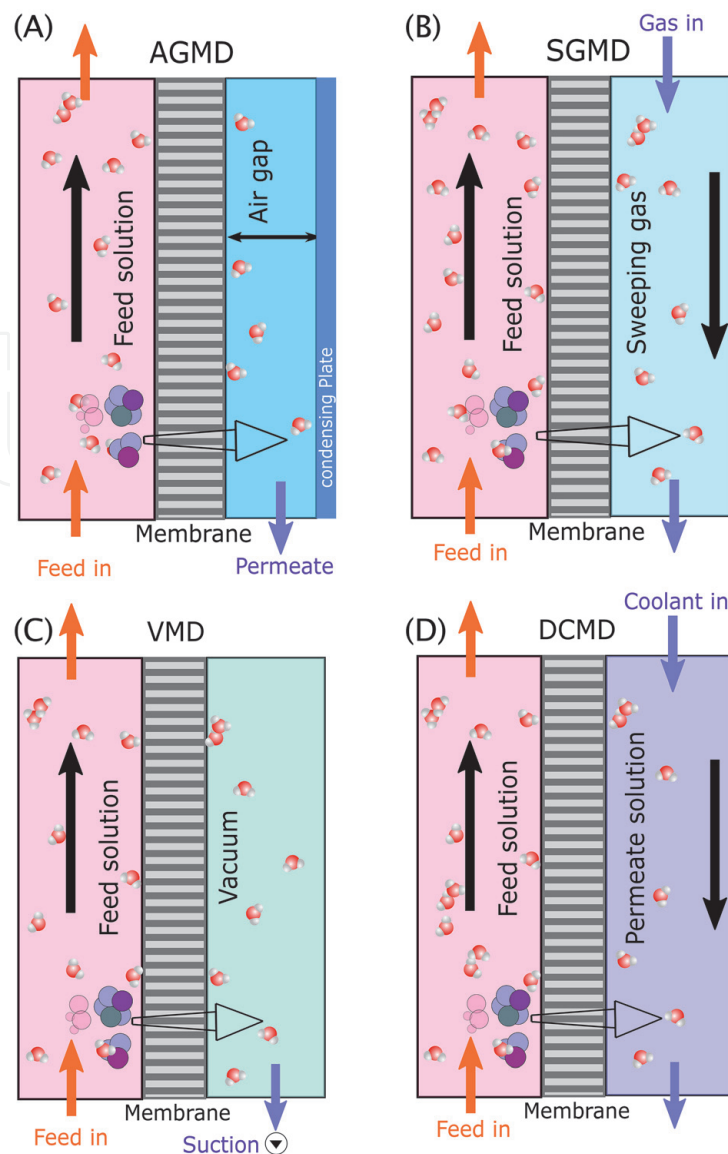


Figure 2.
 A schematic of the four different MD configuration (A–D). The feed water flows tangentially in a cross flow regime at the feed side. At the permeate side, distillate taken off through various mechanisms and membrane allows only vapors to pass through.

gases at the permeate side. The pore wetting possibility is very less as the flow of gas takes off the distillate without condensing it [11]. The main disadvantage of this configuration is the high gas flow to sweep a unit volume of the permeate product. SGMD can be used in desalination and concentration of non-volatile liquids [7, 8].

3. *Vacuum membrane distillation*: The VMD and SGMD are very much similar in stripping out the permeate product. The VMD uses vacuum suction to strip off the vapors from permeate channel and either condense those externally or discarding as waste. **Figure 2(C)** shows a typical VMD configuration. The main advantage of this configuration is to separate the volatile organics from the main stream. However, it requires an additional pump and a condenser, increasing both CAPEX and OPEX. Also, the possibility of wetting the membrane is high due to the negative pressure at the distillate side [5, 8].

4. *Direct contact membrane distillation*: The DCMD is the most widely used MD configurations due to its simplicity, low capital cost and comparatively higher

flux [12–14]. In DCMD, as the name suggests, the membrane remains in direct contact with both solutions, i.e., feed and permeate. **Figure 2(D)** shows a schematic of a typical DCMD set up. The vapors transfer through the membrane and condense in the circulating coolant at the other side of the membrane. To achieve high thermal efficiency, the feed and coolant stream runs in counter-current directions. DCMD is best suited for applications where water is a major permeate, such as desalination and concentration of fruit juices. Also, the condensation step is carried out inside the module itself. High conduction losses across the membrane are the main disadvantage of DCMD [8, 15].

Table 1 summarizes the applications, advantages and disadvantages of different MD configurations [4, 6–9, 11, 15–17].

1.1 Transport phenomena

The temperature gradient between the feed and distillate sides of the MD system result in heat transfer from hot feed to cold distillate accompanied by mass transfer.

1.1.1 Heat transfer

MD is a non-isothermal process. Due to the difference in temperature at feed and permeate sides, three main heat transfer mechanisms take place: convective heat transfer, conduction heat transfer, and latent heat transfer. At the feed side and permeate side, convective and latent heat transfer take place. Across the membrane, conductive and convective heat transfer takes place. The two interfaces show convection with the bulk fluid, and membrane pores demonstrate the conduction phenomenon associated with vapor heat transfer. Due to a positive temperature gradient, it is clear that the heat transfer takes place only from feed to permeate.

MD configuration	Application area	Advantage	Disadvantage
DCMD	<ul style="list-style-type: none">Seawater desalinationIndustrial wastewaterDye effluents	<ul style="list-style-type: none">High distillate fluxSimple design and operation	<ul style="list-style-type: none">High conductive heat lossHigh heat transfer coefficient
AGMD	<ul style="list-style-type: none">Seawater desalinationIndustrial wastewater	<ul style="list-style-type: none">Low conductive lossLow TPLess chances of distillate contaminationHigh thermal efficiency	<ul style="list-style-type: none">Low permeate fluxHigh mass transfer resistance
SGMD	<ul style="list-style-type: none">Brackish water desalinationAzeotropic mixture separationVOC removal	<ul style="list-style-type: none">Low conductive lossLess pore wettabilityNo in-system condensation	<ul style="list-style-type: none">High gas volume needed
VMD	<ul style="list-style-type: none">Seawater desalinationAroma recoveryIndustrial effluentsVOC removal	<ul style="list-style-type: none">Low conductive lossHigh permeate fluxCondensate obtained externally	<ul style="list-style-type: none">Membrane wettingHigh pump powerHeat recovery is difficult

Table 1. Summary of the applications, advantages and disadvantages of different MD configurations [4, 6–9, 11, 15–17].

1.1.1.1 Feed side

At feed side, hot bulk solution come in contact with the MD membrane. Convective heat transfer Q_f ($\text{W}\cdot\text{m}^{-2}$) takes place and can be expressed as per Newton's law of cooling [14]:

$$Q_f = h_f * (T_{fb} - T_{f,m}) \quad (1)$$

Where h_f is the feed convective heat transfer coefficient ($\text{W}\cdot\text{m}^{-2}\text{K}^{-1}$), T_{fb} is the bulk feed solution temperature (K), $T_{f,m}$ is the temperature (K) at feed-membrane interface.

1.1.1.2 Membrane pore

Heat transfer through membrane occurs in two parallel routes: first is latent heat transfer Q_v at pores mouth and second is conduction heat transfer Q_c . The Q_c is the conduction heat loss and does not contributes to the vapor mass. Hence, for an efficient system, it is required to minimize Q_c as low as possible. It can be expressed by the Fourier's law of conduction. Therefore, thicker membrane contributes less to conduction heat transfer. The Q_m ($\text{W}\cdot\text{m}^{-2}$) is the sum of both heat transfers and can be expressed as [2, 5]¹:

$$Q_m = Q_c + Q_v = \frac{k_m}{\delta_m} * (T_{f,m} - T_{p,m}) + J * h_{fg} \quad (2)$$

$$h_m = \frac{k_m}{\delta_m} \quad (3)$$

Where Q_c is the conduction heat transfer ($\text{W}\cdot\text{m}^{-2}$), k_m is the membrane thermal conductivity ($\text{W}\cdot\text{m}^{-1}\cdot\text{K}^{-1}$), δ_m is the membrane thickness (m), J is the distillate flux ($\text{kg}\cdot\text{m}^{-2}\text{h}^{-1}$), h_{fg} is the latent heat of evaporation ($\text{kJ}\cdot\text{kg}^{-1}$), $T_{p,m}$ and $T_{f,m}$ are the temperature of permeate-membrane interface and feed-membrane interface respectively.

The thermal conductivity k_m ($\text{W}\cdot\text{m}^{-1}\text{K}^{-1}$) of the membrane can be calculated from the thermal conductivity of vapor k_g and the polymer material k_p as per following relations [18]:

$$k_m = \varepsilon k_g + (1 - \varepsilon)k_p \quad (4)$$

Where ε is the porosity of the membrane.

1.1.1.3 Permeate side

Vapor that pass through membrane pores condense at the permeate side at the expense of latent heat of condensation. The heat transfer at the permeate side Q_p ($\text{W}\cdot\text{m}^{-2}$) can be expressed as [15, 18]:

$$Q_p = h_p * (T_{pb} - T_{p,m}) \quad (5)$$

¹ The influence of mass transfer on heat transfer was ignored.

Where h_p is the permeate convective heat transfer coefficient ($\text{W}\cdot\text{m}^{-2}\text{K}^{-1}$), T_{pb} is the bulk permeate solution temperature, $T_{p,m}$ is the temperature (K) at permeate-membrane interface.

1.1.1.4 Overall heat transfer

At steady state, heat transfer from feed to membrane, across the membrane and from membrane to permeate are equal. **Figure 3** shows with the electrical analogy of local heat transfer coefficients and their relationship with the overall heat transfer coefficient. The overall heat transfer Q ($\text{W}\cdot\text{m}^{-2}$) can be expressed in terms of universal (overall) heat transfer coefficient as U [2, 18]

$$\begin{aligned} Q &= Q_f = Q_m = Q_p \\ &= h_f * (T_{fb} - T_{f,m}) = \frac{k_m}{\delta_m} * (T_{f,m} - T_{p,m}) + J * h_{fg} = h_p * (T_{pb} - T_{p,m}) \quad (6) \\ &= U * (T_{f,m} - T_{p,m}) \end{aligned}$$

Where U ($\text{W}\cdot\text{m}^{-2}$) can be expressed as:

$$\frac{1}{U} = \frac{1}{h_f} + \frac{1}{\frac{k_m}{\delta_m} * \frac{J h_{fg}}{(T_{f,m} - T_{p,m})}} + \frac{1}{h_p} \quad (7)$$

The membrane interface temperatures, i.e. $T_{f,m}$ and $T_{p,m}$ can not be measured experimentally. Therefore, mathematical iterative procedure is generally used to evaluate both interface temperatures. The membrane interface temperature can be derived from the Eq. (6) and expressed as [15, 19]:

$$T_{f,m} = T_{fb} - \frac{J h_{fg} + \frac{k_m}{\delta_m} (T_{f,m} - T_{p,m})}{h_f} \quad (8)$$

$$T_{p,m} = T_{pb} - \frac{J h_{fg} + \frac{k_m}{\delta_m} (T_{f,m} - T_{p,m})}{h_p} \quad (9)$$

The heat transfer coefficients h_f and h_p can be calculated using Nusselt number relation as shown in Eq. (10), while the h_m can be calculated from Eq. (3). The Nusselt number correlations are available in the literature [2, 4, 5].

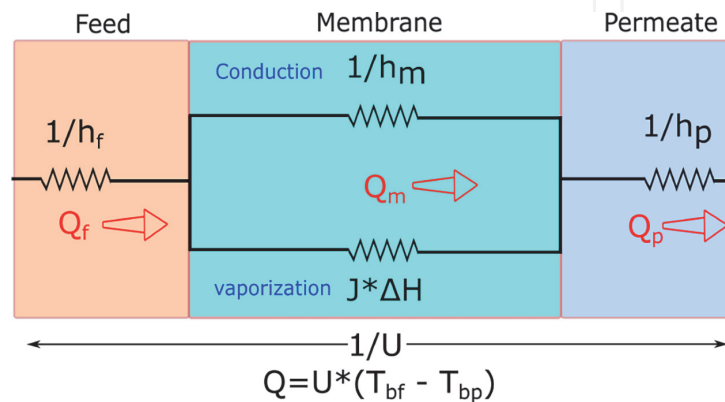


Figure 3.

Electrical equivalent of heat transfer resistance in MD process. An overall heat transfer resistance is an equivalent of all three heat transfer resistance of feed, membrane and permeate.

$$\text{Heat transfer coefficient} = \frac{Nu * k_m}{D_p} \tag{10}$$

Where h_m is defined in Eq. (3)

1.1.2 Mass transfer

Mass transport in MD can be explained by three sequential stages: vapor generation, vapor transport, and vapor condensation, which respectively take place at the feed-membrane interface, membrane pores, and permeate-membrane interface. **Figure 4** shows the mass transfer process, including vapor generation at the feed side, vapor transport through the porous membrane, and finally, vapor condensation at the permeate side. There is resistance to mass transfer at each stage, which is defined by a correlation explained in the sequel. The overall mass transfer in the MD system is often expressed using Darcy’s law i.e., the vapor pressure difference between two sides of the membrane, and is given as [1, 2]:

$$J = C_m * (p_{f,m} - p_{p,m}) \tag{11}$$

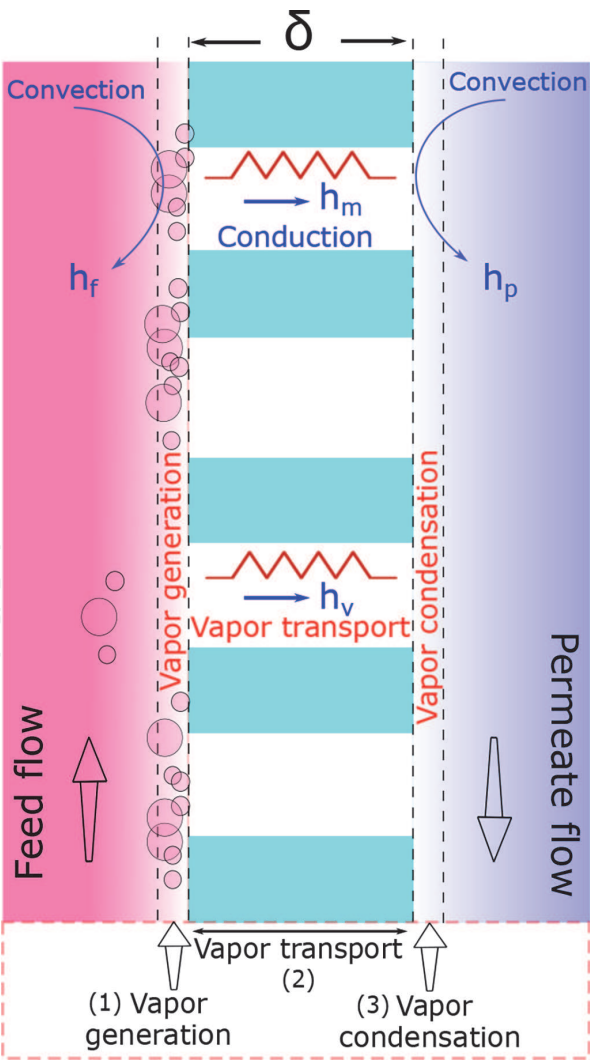


Figure 4. A schematic of vapor transfer from vapor generation at the feed side, to the permeate side through the membrane pores. Mass transfer is the transport mechanism within the membrane pores. Finally, the distillate condenses at the permeate side.

Where C_m is the membrane mass transfer coefficient ($\text{kg} \cdot \text{m}^{-2} \cdot \text{h}^{-2} \cdot \text{Pa}^{-2}$), p_f and p_p are the partial pressures of water at feed and permeate sides, respectively. The three stages of mass transport are explained as below:

1.1.2.1 Stage 1 (Vapor generation)

At the feed side of the membrane, liquid feed remains in contact with the membrane pores. The vapors are generated at the feed-membrane pore interface when the hot feed solution passes over the hydrophobic MD membrane. The partial pressure of the vapor generated is directly proportional to the temperature as per Antoine's equation [19]. In the case of water, Antoine equation can be rewritten as Eq. (12):

$$p_v = \exp \left[23.19 - \left(\frac{3816.44}{T_{f,m} - 46.13} \right) \right] \quad (12)$$

where p_v is the vapor pressure of water (Pa) and $T_{f,m}$ is the temperature at the feed-membrane interface (K).

The presence of non-volatile solute in the feed water decreases the vapor pressure of the feed solution. Therefore, the vapor pressure is a function of mole fraction of that component and can be expressed as [4]:

$$p_{(x)} = (1 - x_s) * p_w^o \quad (13)$$

Where x_s mole fraction of non-volatile solute in feed water and p_w^o is the partial pressure of pure water.

Figure 5 shows a control volume of heat and mass transfer of length dz . A feed of mass flow rate \dot{m} fed into the feed channel, and heat and mass transfer takes place along the membrane surface. The width dy is taken as unity. The mass balance at feed side can be explained mathematically as [13, 20]:

$$\dot{m}_{f,(z+dz)} h_{fb} = \dot{m}_{f,(z)} h_{fb} - (J h_{fg} + q_m) dA \quad (14)$$

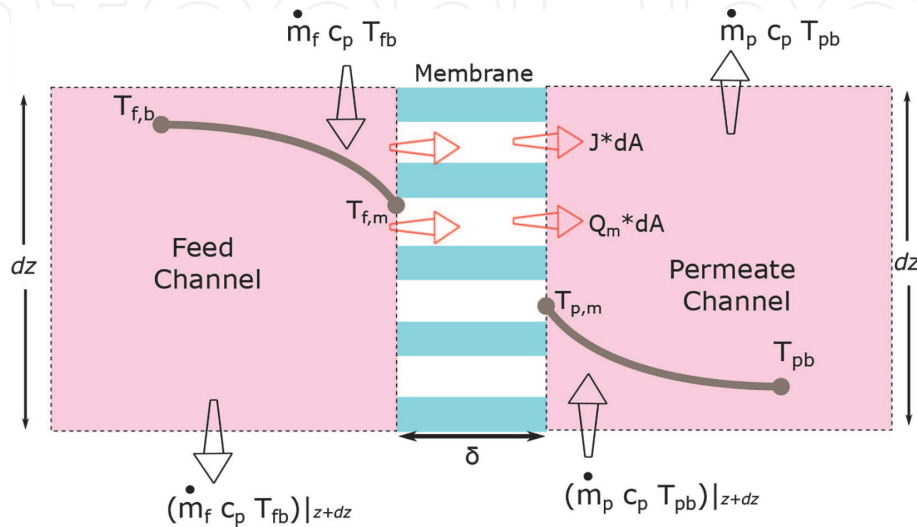


Figure 5. A schematic of the mass balance in a control volume at the feed side and permeate side. The mass transfer takes place through the porous membrane along the vapor pressure gradient.

The mass flux of water that passes through the membrane can be expressed as:

$$J = k_f \rho_f \ln \frac{x_{f,m}}{x_f} \quad (15)$$

Where k_f is the mass transfer coefficient and can be calculated using Sherwood number as follow [4]:

$$Sh = \frac{k_f d_h}{D_s} \quad (16)$$

Where d_h is the hydraulic diameter (m), D_s is the solute diffusion coefficient in bulk feed ($\text{m}^2 \cdot \text{s}^{-1}$). The Sherwood number can be calculated using following semi-empirical relationship [4]:

$$Sh = \alpha Re^\beta Sc^\gamma \quad (17)$$

Where α , β , and γ are the coefficients calculated from experiments. Sc is the Schmidt number and Re is the Reynolds number, which can be expressed as [2]:

$$Sc = \frac{\eta_f}{\rho_f D_s} \quad (18)$$

$$Re = \frac{\rho_f v_f d_h}{\eta_f} \quad (19)$$

Where η_f is the viscosity of the bulk fluid ($\text{Pa} \cdot \text{s}$), ρ_f is the density of the bulk fluid ($\text{kg} \cdot \text{m}^{-3}$), and v_f is the fluid flow velocity ($\text{m} \cdot \text{s}^{-1}$). Different correlations used for Sherwood number are listed in Appendix 1A.

1.1.2.2 Stage 2 (Vapor transport)

Two major factors control the vapor transfer in MD membrane pores. One is the vapor pressure difference Δp , and the second is the mass transfer coefficient of the membrane. The vapor transfer through the membrane may be the limiting step for mass transfer in MD, which is influenced by the physical properties of the membrane and other characteristics which expresses with the relation $J \propto \frac{D_p}{\chi} \frac{\epsilon}{\delta_m}$ [1].

1. *Porosity* (ϵ): In general, regardless of the type of MD configuration, membranes with high porosity have more distillate flux as well as lower conductive heat loss. The porosity of MD membranes lies between 30 and 85% [4, 21].
2. *Tortuosity* (χ): In a simple assumption, membrane pores are considered as straight cylindrical channels. However, they possess many curved paths. High tortuosity value leads to lower distillate flux due to vapor permeation through tortuous paths. Therefore, membrane permeability is inversely proportional to the membrane tortuosity. In most theoretical models in MD studies, a tortuosity value of 2 is frequently considered to predict the transmembrane flux [15].
3. *Pore size*: Large pore size allows more vapor to pass through. However, after a certain point, it will limit the applied pressure to avoid pore wetting. On the other hand, small pore size enables working at high pressures but at the cost of lower fluxes [4].

The vapor transport mechanism through MD membrane pores is governed by three basic mechanisms known as Knudsen diffusion (K_n), Molecular-diffusion, and viscous (poiseuille flow). The mass transport through the membrane is described by the simple Darcy's law, expressed in Eq. (11). For dilute solutions, it can be written as [7, 22]:

$$J = C_m * \frac{dP}{dT} (T_{f,m} - T_{p,m}) \quad (20)$$

The Pressure term $\frac{dP}{dT}$ can be calculated from Clausius-Clapeyron equation as:

$$\frac{dP}{dT} = \frac{\Delta H}{RT^2} P_{av}(T_m) \quad (21)$$

The pressure P_{av} for non-ideal aqueous solution can be calculated from Raoult's law as expressed by Eq. (13).

As per Darcy's law Eq. (11), membrane mass flux is mainly governed by the partial pressure difference between feed and permeate side and the membrane mass transfer coefficient C_m . The membrane mass transfer coefficient is primarily a function of membrane properties (thickness, pore size, tortuosity) and the process conditions (temperature and pressure). Its value depends upon the mass transfer mechanism inside the membrane pore.

The air molecules (particles) act as a medium in the pores. Knudsen number (K_n) determines the type of governing mechanism of mass transport inside the membrane pore and can be expressed as [1]:

$$K_n = \frac{\lambda}{D_p} \quad (22)$$

Where D_p is the pore diameter (m) λ is the mean free path (m) of the vapor molecule and can be written as [19]:

$$\lambda = \frac{k_B T_r}{\sqrt{2} \pi P_m \sigma_v^2} \quad (23)$$

where k_B is the Boltzmann constant ($1.38 \times 10^{-23} \text{ J} \cdot \text{K}^{-1}$), P_m is the mean average pressure in membrane pores (Pa), T_r is the average temperature in the pore, and σ_v is the water vapor collision diameter (0.2641 nm).

Depending on the value of K_n , three possible mass transfer modes exist as follows: (a) Knudsen diffusion ($K_n > 1$) in which molecular collisions with the walls dominate as compared to the molecule-molecule collisions, (b) molecular diffusion ($K_n < 0.01$) in which the frequency of gas molecule collisions is much higher than those with the pore walls, and (c) Knudsen-molecular diffusion ($0.01 < K_n < 1$) in which the frequency of molecular collisions with the pore walls is similar to that of the gas-gas collisions (often referred to as "transitional regime") [4, 19]. **Figure 6** shows a schematic of three possible mass transfer mechanisms through the pores of an MD membrane.

- i. *Knudsen diffusion*: If the mean free path of water molecules is greater than the pore diameter ($\lambda > D_p$), the frequency of collision between water molecules are less than the molecule-pore wall. The Knudsen number in this regime is ≥ 1 [19]. Therefore, it is the dominating process of mass transport in DCMD. The mass transfer resistance arises from the momentum transfer of vapor molecules with the sidewalls of the pores.

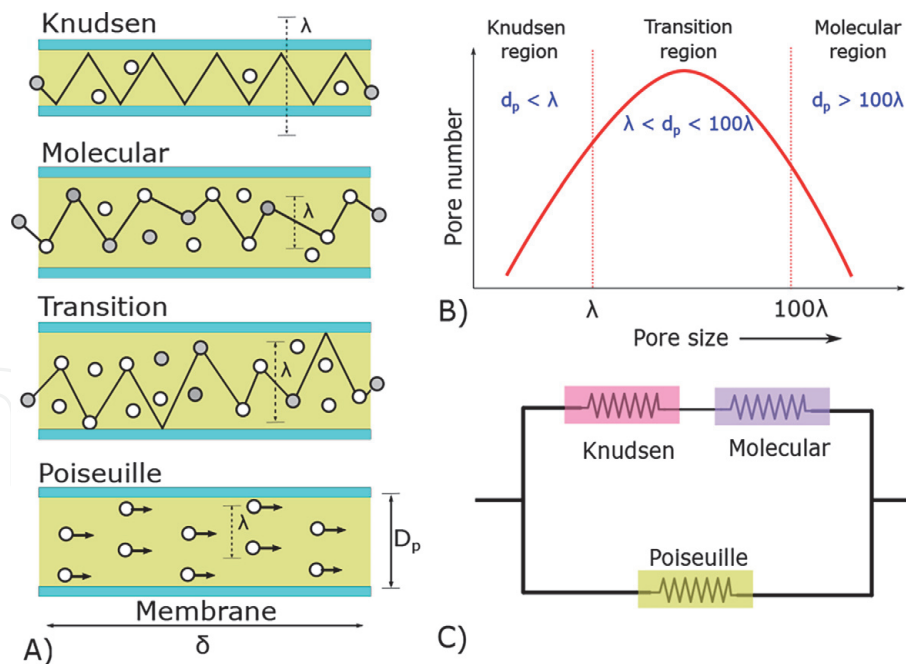


Figure 6.
(A) Various mechanisms of vapor transport through membrane pores are shown. (B) Mass transport regime based on the pore size. The transition regime occurs in the intermediate values of the Knudsen number. (C) Mass transport resistance and their electrical circuit analogy.

Therefore, Knudsen diffusion decreases with the increase of temperature. In this case, the membrane mass transfer coefficient is shown in **Table 2**.

- ii. *Molecular diffusion*: Molecular diffusion occurs when the mean free path of vapor molecule ($\lambda < D_p$) is much shorter than the pore diameter. The Knudsen number in this case is below 0.01 [5, 7]. Therefore, the intramolecular (within own molecules) and intermolecular (with the air molecules) collisions prevail vapor molecule-wall collisions. The mass transfer resistance comes from the collision of vapor molecules with the air molecules entrapped inside the membrane pores. In this case, the membrane mass transfer coefficient and mass transfer mechanism are shown in **Table 2** and **Figure 6** respectively. Since the feed and permeate in DCMD is deaerated, therefore, molecular diffusion in DCMD is minimum [2]. Similarly, in the case of VMD, the vacuum in the permeate side remove the entrapped air in the pore. Therefore, molecular diffusion is neglected there as well.
- iii. *Poiseuille flow*: In poiseuille flow (viscous flow), vapor molecule acts as a continuous fluid flow under a pressure gradient between two sides of membrane. It occurs in deaerated membrane pores under a stream vacuum. It applies when the mean free molecular path of vapor molecule is smaller than the pore size ($d_p > 100\lambda$) [2, 25]. The membrane mass transfer resistance is due to momentum transfer to the pore walls through viscous drag and its coefficient is shown in **Table 2**.
- iv. *Knudsen-molecular diffusion*: Transport of water vapors is a complex phenomenon and can encounter mass transfer resistance from both air molecule and the pore walls. In practical, there exist more than one type of transport phenomenon, therefore, called transition flow. This type of transport occurs when the mean free path of the vapor molecule is in the range $(1-100)\lambda$ and the flow is a kind of transition flow between pure

Knudsen number	Type of transport	Condition	Mass transfer coefficient C_m
> 1	Knudsen diffusion	$\lambda > > D_p$	$\frac{2}{3} \frac{\varepsilon}{\chi} \frac{r}{\delta} \sqrt{\frac{8}{\pi} \frac{M_w}{R T}}$
$0.01 - 1$	Knudsen-molecular diffusion	$\lambda < D_p < 100\lambda$	$\left[\left(\frac{\chi}{\varepsilon} \delta * \frac{R T_m P_a}{M_w P_T D_w} \right) + \left(\frac{(3 \chi \delta)}{(2 \varepsilon r)} \sqrt{\frac{\pi R T}{8 M_w}} \right) \right]^{-1}$
< 0.01	Molecular diffusion	$\lambda < < D_p$	$\left(\frac{\varepsilon}{\chi} \delta \frac{M_w}{R T_m} \frac{P_T}{P_a} (D_w) \right)$
< 0.01	Poiseuille flow	$\lambda < < D_p$	$\left(\frac{1}{8} \frac{r^2}{\chi} \frac{\varepsilon}{\delta} \frac{M_w}{R T_m} P_m \right)$

Table 2. Mass transfer mechanism within the membrane pores follow a specific regime based on the Knudsen number. The mass transfer coefficient (C_m) of each mechanism is shown [1, 2, 4, 5, 19, 23, 24].

Knudsen, and molecular diffusion [5]. The membrane mass transfer coefficient is shown in **Table 2**.

1.1.2.3 Stage 3 (Vapor condensation)

At permeate side, each configuration of MD uses different methods to collect permeate. In some cases, the permeate is the waste and is discarded, while in other instances, permeate is the product and collected using various methods based on the configuration. In DCMD, the permeate is stripped by circulating pure water. Therefore, it offers no mass transfer resistance. In the case of VMD, the presence of vacuum also negates the existence of mass transport resistance.

However, AGMD show a significant resistance due to the presence of an air gap between the membrane and the condensing plate. In AGMD, the mass transfer occurs through molecular diffusion between the membrane pore surface to the condenser plate. The mass transfer resistance can be expressed by:

$$k_s = \frac{P_{av}}{P_a} \frac{\varepsilon}{\delta} \frac{D_w}{\gamma + b} \frac{M_w}{R T_m} \tag{24}$$

Where b is the thickness of the air gap (m) [2, 4].

1.1.3 Temperature polarization

The phenomenon of evaporation at the feed-membrane interface and condensation at the permeate-membrane interface creates a temperature gradient with the bulk solution. Temperature polarization (TP) is a condition when the temperature at the membrane interface differs from its bulk solution [26–28]. TP is considered a critical factor that impacts the vapor flux of an MD system. The evaporation phenomenon at the liquid-air interface draws the latent heat from the bulk solution. Similarly, at the permeate side, the liquid-membrane interface releases heat of condensation to the coolant liquid. This creates a temperature difference between the bulk solution and the membrane interface. **Figure 7** shows a schematic representation of temperature profile across the membrane [28].

There exist a thermal boundary layer at each side of the membrane. However, this thermal boundary layer does not have a significant effect in the case of AGMD, VMD, and SGMD. Moreover, the salt concentration at the feed-membrane interface increases due to mass transfer, leading to the concentration polarization (CP) phenomenon. However, the effect of CP is negligible in MD [18, 29]. The operation parameters such as fluid velocity, concentration, and temperature of feed solution

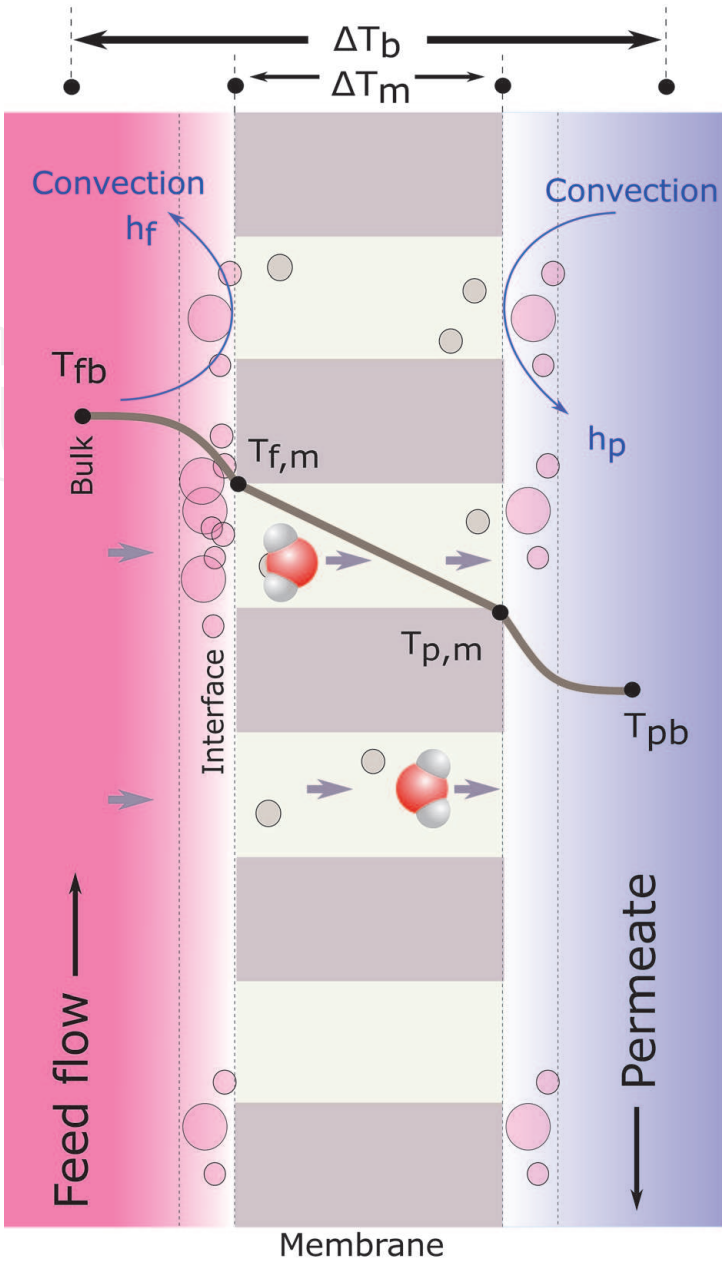


Figure 7.
A profile of temperature deviation at interfaces with the bulk fluid on both sides of the membrane. The temperature change at the membrane interface ΔT_m and bulk ΔT_b is shown to determine the polarization coefficient.

affect the TP. Higher velocity increases the heat transfer by creating turbulences locally, hence diminishing the thermal boundary layer. Additionally, the lower concentration and higher temperature of the feed solutions produce high vapor pressure as per Rault's law and Antoine's Eq. (12) respectively. All the above parameters decrease the effect of TP. In addition, the membrane also plays an important role in TP due to the heat transfer across it. High porosity decreases the TP, while higher thermally conductive polymers show high TP. However, high thickness decreases the heat loss across the membrane as per Fourier's law Eq. (2) and hence decreases TP. It is observed that TP decreases the vapor flux significantly [21].

1.1.3.1 Temperature polarization coefficient

The quantification of TP is expressed in temperature polarization coefficient (TPC). **Figure 7** shows the temperature difference at the membrane interfaces with its bulk. TPC represented as Θ is expressed as [19]:

$$\Theta = \frac{\Delta T_m}{\Delta T_b} = \frac{(T_{f,m} - T_{p,m})}{(T_{fb} - T_{pb})} \quad (25)$$

The thermal boundary layer at both sides of the membrane acts as resistances to heat transfer. In other words, TPC is the ratio of thermal boundary layer resistance to the total heat transfer resistance. In the case of VMD, TPC can be simplified as the ratio of feed-membrane interface temperature to the bulk feed temperature [1], as expressed in Eq. (26).

$$\Theta = \frac{T_{f,m}}{T_{fb}} \quad (26)$$

The TPC value, lies between 0–1 and most of the literature reports results between 0.4 and 0.7 [1, 3, 5, 30]. When the TPC value approaches zero, the system is limited by heat transfer at the feed side, which indicates an inefficient design. In contrast, TPC value 1 indicates that the system is affected by mass transfer resistance.

Several studies have been proposed to mitigate TP by using turbulence promoters such as spacers. However, this approach creates additional energy requirements [27, 31–34]. Considering that TP and conduction heat loss is an intrinsic process deficiency that cannot be fully mitigated, it is highly desirable to seek alternative approaches to alleviate heat loss and achieve a sustainable MD performance.

2. Parameters that affect MD vapor flux

Most of the MD research is focused on maximizing vapor flux. However, taking vapor flux as a matrix to evaluate the thermal performance, may not be a correct approach since vapor flux depends upon many factors including MD system configurations, active membrane area, type of energy input, heat recovery from exiting feed etc. Therefore, the highest flux may not lead to the best thermal efficiency. Following are the parameters affecting the vapor flux:

1. *Effect of feed temperature:* The feed temperature is the most important factor and has a major effect on the vapor flux of an MD system. An exponential increase in vapor flux was observed with the increase in inlet feed temperature. This is due to the exponential increase of vapor pressure with temperature resulting in increase in driving force. **Figure 8** shows the effect of feed temperature on permeate vapor flux on DCMD.

Further, the conduction heat transfer is also higher at higher feed temperatures, leading to higher temperature polarization. Though, at high inlet feed temperature, the thermal efficiency is higher due to higher vapor flux, as shown in the **Figure 8**.

2. *Effect of permeate temperature:* In most of lab scale MD systems, the permeate temperature varies from 10 to 40°C. Increase in permeate temperature resulted in decrease in trans-membrane driving force, hence, vapor flux decreases. The effect varies from linear to exponential depending upon the membrane module characteristics [15, 35].
3. *Effect of feed and permeate flow rate:* The feed and permeate velocity influence the temperature polarization by creating the hydraulic turbulences in the feed

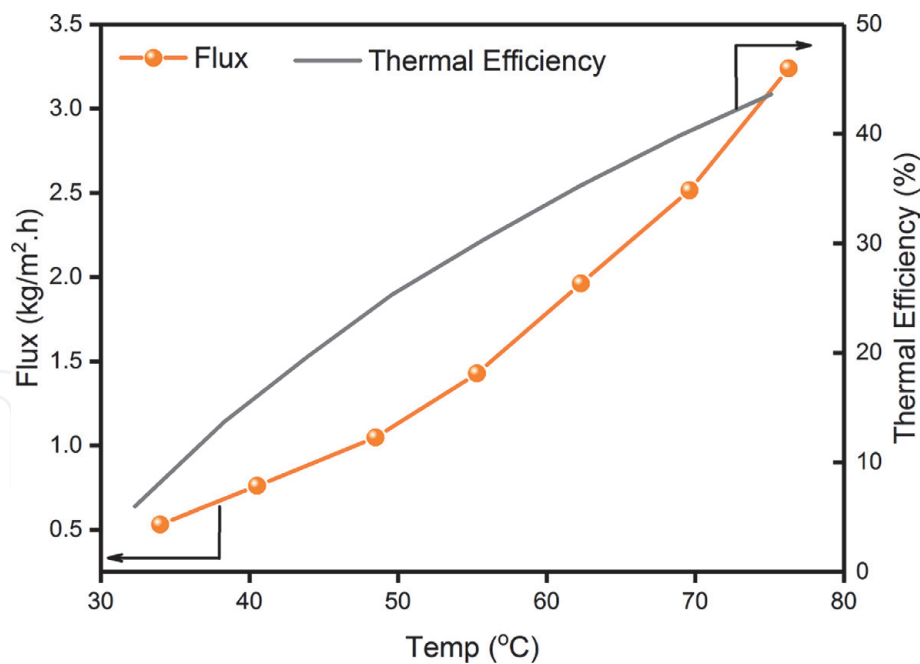
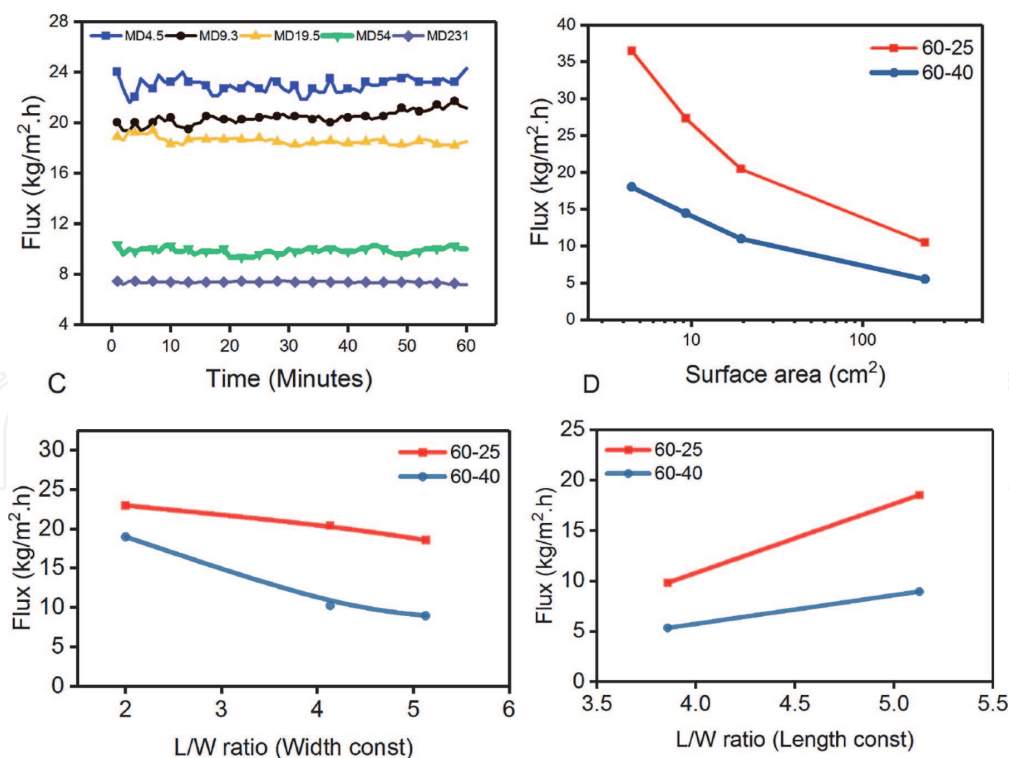


Figure 8.
 Graph showing temperature effect on vapor flux of a DCMD configuration. The Line graph shows the variation in thermal efficiency with feed inlet temperature. Adapted from [15].

and permeate channel respectively. The turbulences increase the heat and mass transfer coefficient (h_f, h_p) at the MD membrane's feed and permeate boundary layer. The increased flow rate decreases the effect of concentration polarization. The vapor flux increases to an asymptotic value with an increase in feed velocity. Further, the thermal boundary layer thickness decreases at higher feed velocities. Kubota et al. (2020) revealed that the permeate flux increases with the feed velocity until it reaches a maximum and then decreases [7, 36].

4. *Effect of the presence of non-condensable gasses:* Non-condensable gasses such as CO_2 present in the feedwater stream. These gasses may mask the membrane pores, producing mass transfer resistance. Feedwater is generally aerated with N_2 gas before feeding in the MD system. However, this effect does not affect the VMD process. The process of deaeration consumes energy, and hence it decreases the overall performance [36].
5. *Effect of solute concentration:* High salt concentration decreases the vapor flux due to decrease in vapor pressure as per Roults law. Additionally, concentration polarization may develop at the vicinity of the membrane, producing mass transfer resistance. A reduction in coefficient of polarization (θ) and thermal efficiency were observed with the increase in salt concentration [37]. Martinez et al. demonstrated that vapor flux decreased only by 1.15 fold by increasing the salt concentration by fivefold [38]. Therefore, MD can be used to treat high saline water with a slight decrease in productivity [1, 39].
6. *Effect of module geometry:* The configuration arrangement and the modular dimensions affect the TP in an MD system. Longer channel (keeping the width constant) leads to higher water production capacity, however, the flux decreases due to continuous decrease in feed water temperature along the length. The higher water production capacity is due to high water residence time with the MD membrane [40].

**Figure 9.**

Vapor flux variation with respect to the modular dimensions of various MD flow cell sizes.

As the feed water moves along the length (with constant width), it loses heat due to latent heat and heat of conduction, which results in temperature decrease. Therefore, the permeate flux decreases. However, due to more residence time, the total water capacity increases. Therefore, there is an optimum length of the feed channel length. The water flux variation with the length, length/width ratio, surface area have been investigated to underline the affect. [40] presented a mathematical model simulation which shows that the total residence time of feed water in the feed channel has a positive effect until a limit, after that it started decreasing. The peak of the curve shows the optimum length of the feed channel.

Figure 9 shows the vapor flux data of four MD module types having surface area 4.5, 9.3, 19.5, 54, and 231 cm^2 . The vapor flux was plotted with various variables. **Figure 9(A)** It is observed that the small active surface area membranes performance is higher than large surface area. This was a general consideration because the MD types were of different length and width. This can be deduced that regardless of width and length, the flux of lower active membrane surface area is higher than the larger ones, which is shown in the **Figure 9(B)**. This shows a negative exponential correlation of the flux with the surface area.

The length has a negative effect on the vapor flux as demonstrated in a simulation by Lee et al. [40]. Our experimental data verifies this relation as shown in **Figure 9(C)**. If the length was kept constant, increasing the width was a positive effect on vapor flux [40]. The length to width ratio versus flux is plotted in the **Figure 9(D)** shows a positive slop.

As the length increases, the temperature of the feed drops due to the effect of latent heat and conduction heat loss along the length. The temperature drop increases. This was confirmed by the simulated results demonstrated by [40].

3. Membrane properties

Unlike Reverse Osmosis, MD membranes are not chemically involved in the mass transfer phenomenon. However, they are involved in the heat transfer

phenomenon. MD membranes require some specific physical and chemical characteristics to perform well in the MD process. Mainly two types of membranes are used: Polyvinylidene Fluoride (PVDF) and Polytetrafluoroethylene (PTFE). **Figure 10(A)** shows the required characteristics of an ideal MD membrane, and **Figure 10(B–C)** shows an SEM topography of typical PVDF and PTFE membranes. PVDF membranes have round pores that could be seen on the top surface, while PTFE has pores strangled between the polymer fibers. The required physical and chemical characteristics of an MD membrane include:

1. *High Porosity (ϵ)*: Membrane porosity is the volume of pores to the total volume of the membrane. Membranes with high porosity produce more distillate flux due to more available channels for mass transfer and lower conductive heat loss. However, it decreases the mechanical strength and make membrane prone to crack under mild pressure. Porosity of MD membranes lies between 30 and 85% [21].
2. *Adequate thickness (δ_m)*: The membrane thickness offsets both membrane permeability and heat transfer. Thicker membranes are suitable to prevent heat loss but will affect water vapor permeability [21].
3. *Lower tortuosity (χ)*: Tortuosity is the deviation of pores from a straight cylindrical path in porous media. In a simple assumption, membrane pores can be considered as straight cylindrical. However, this assumption is often far from reality. High tortuosity values lead to lower distillate flux due to vapor permeation through tortuous paths. Therefore, membrane permeability is in inverse relation to membrane tortuosity. In most theoretical models in MD studies, a value of 2 is frequently considered to predict the transmembrane flux [15].

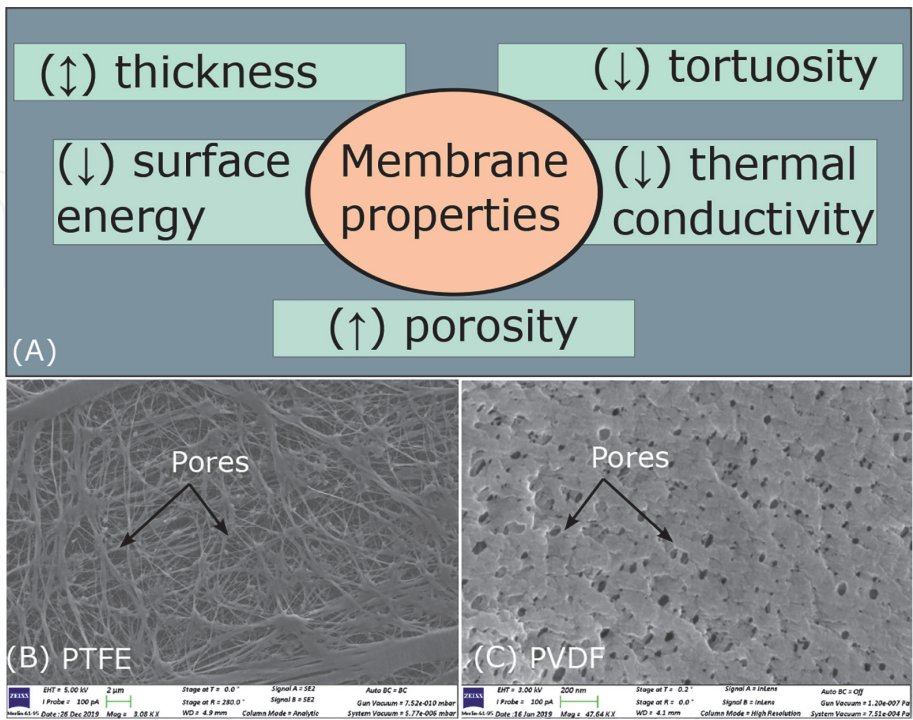


Figure 10.
(A): The typical characteristics of an ideal MD membrane. (B–C): A surface topography of PTFE and PVDF membranes through SEM imaging. The pores in a typical PVDF and PTFE membranes are also depicted.

4. *Low thermal conductivity (k_m):* The high thermal conductivities facilitate sensible heat transfer, which leads to a decrease in temperature difference across the two sides of the membrane. Hence, vapor flux decreases. Therefore, low thermal conductivity is desired for MD membranes [22].
5. *Low surface energy:* Low surface energy correlates with high hydrophobicity. Materials with high hydrophobicity can transform to membranes with larger pores, which eventually increases the vapor flux. Also, high hydrophobic materials allow membrane processes to operate at high pressure for a given pore size [22].

3.1 MD module design

DCMD is one of the most used MD configurations due to its simplicity. Different MD modules have been developed to address a variety of process requirements. Based on membrane type and design principle, MD modules have been developed into three different designs:

1. **Flat sheet module:** In the flat sheet module, a flat sheet membrane is put tangentially with the feed flow. Flat sheet membranes offer simple fabrication and assembly, easy cleaning and maintenance. The main disadvantages of the flat sheet are its low packing density, and high propensity to wetting [41].

Figure 11(A) shows a typical set up of flat sheet DCMD.

2. **Hollow fiber module:** In this type of module, hollow fiber membranes are used. Membranes are set in parallel bundles in the shell of a cylindrical casing. The main advantage of the hollow fiber module is the high packing density (surface area to volume ratio) and lack of membrane support. However, the

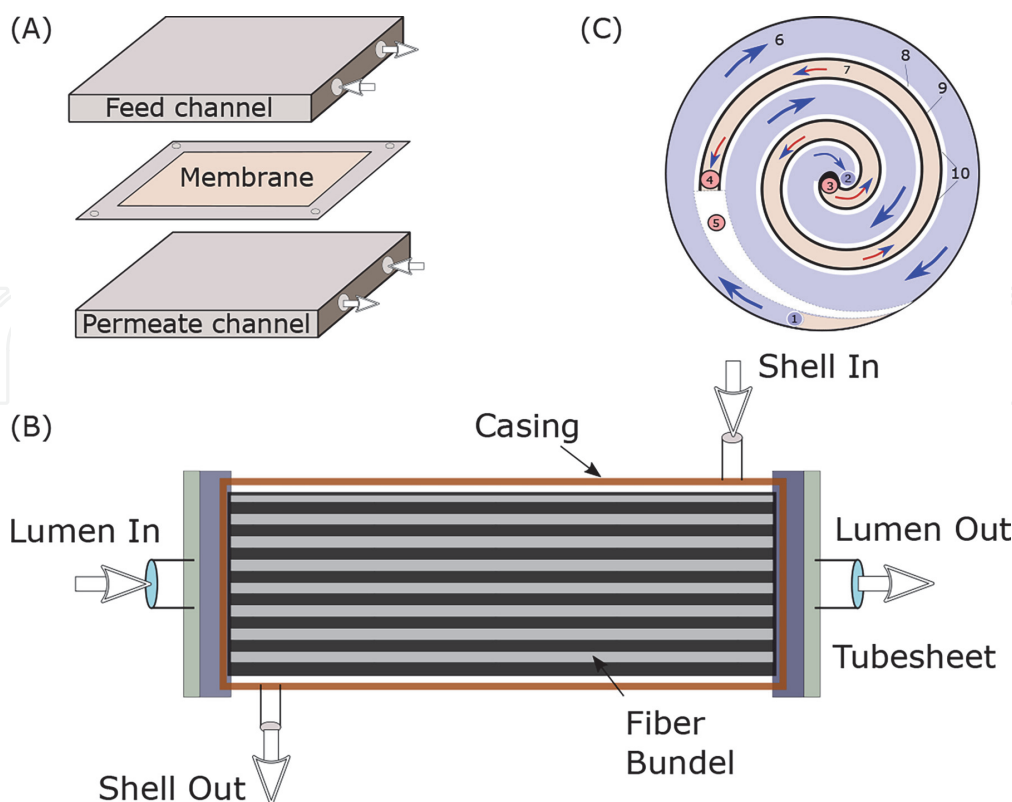


Figure 11.

(A): Flat sheet membrane module, showing a rectangular membrane between two channels. (B): A schematic of Hollow Fiber module set up, comprising hollow fiber membrane cased in a housing. (C): A spiral wound DCMD module commercialized by Solar Springs, adapted from [42].

permeate flux of the hollow fiber module is lower to that of the flat sheet. Additionally, the cleaning process and the membrane replacement is difficult in the hollow fiber module [4, 41]. **Figure 11(B)** shows a typical set up of hollow fiber DCMD.

3. **Spiral wound:** Flat sheets are spirally coiled in a cylindrically wound shape. The membrane is rolled with the spacer between the feed and coolant fluids, creating evaporator and condenser channels. Such type of system was first commercialized by Solar Springs as Oryx unit as shown in **Figure 11(C)** [42]. The condensation process first preheats the cold feed as a condenser stream in the spiral wound design. Then, preheated feed is heated to a required temperature before entering from its center. The feed solution flows axially in the evaporator channel, and the permeate which passes through the membrane flows spirally. The condenser channel is placed toward the shell side while feed towards the core side to get the advantage of counter-current circulation [6].

4. Performance evaluation

The MD performance metrics can be divided into two thermodynamic categories: local and system level. Local metrics are impacted by local properties such as porosity, pore size, thickness, membrane conductivity etc. These include permeate flux and thermal efficiency. On the other hand, the system-level metrics are impacted by the process parameters such as temperature, energy flow, etc. These can be divided into first law efficiencies (GOR, SEC) and second law efficiencies (thermal efficiency-II) [43]. In the context of MD, these can be described as follows:

1. **Permeate flux:** The permeate flux J ($\text{kg} \cdot \text{m}^{-2} \cdot \text{h}^{-2}$) is the amount of distillate transported through a unit membrane area. It is the most significant parameter to evaluate the performance of an MD system. It can be expressed as:

$$J = \frac{\dot{m}_d}{A_m} \quad (27)$$

Where A_m is the active surface area (m^2) of the membrane, and \dot{m}_d is the amount of distillate that passes through the membrane ($\text{kg} \cdot \text{s}^{-1}$).

2. **Gained output ratio:** Gained output ratio (GOR) is the first law efficiency of a thermal desalination system and is often used to quantify energy efficiency. It is defined as the ratio of thermal energy required to vaporize the distillate mass to actual heat input. Mathematically, it can be expressed as [44, 45]:

$$\text{GOR} = \frac{\dot{m}_d * h_{fg}}{Q_{in}} \quad (28)$$

Where

$$Q_{in} = \dot{m}_f * c_p * \Delta T_{12} \quad (29)$$

Where c_p is the specific heat capacity of fluid ($\text{Jkg}^{-1}\text{K}^{-1}$). For a system, with no heat energy recovery, GOR is simply a thermal efficiency without a heat exchanger. The GOR is a dimension-less quantity and its value lies between 0 and 1 for a single pass system without any heat recovery, and more than 1 if

the evaporation and condensation heat is reused. In other words, GOR tells how many times the enthalpy of evaporation is reused. For most of the commercial systems and large distillation units, the condensation heat is utilized, therefore, shows values greater than 1.

3. *Specific energy consumption*: Specific energy consumption (SEC) is the energy consumed to produce a unit amount of distillate volume [42, 44, 46]. It is expressed as:

$$SEC = \frac{Q_{in}}{m_d} = \frac{\dot{m}_f * c_p * \Delta T_{12}}{m_d} \quad (30)$$

Where \dot{m}_f , c_p , ΔT_{12} , Q_{in} , and m_d are the mass flow rate of feed solution ($\text{kg}\cdot\text{s}^{-1}$), specific heat of water ($\text{kJ}\cdot\text{kg}^{-1}\text{K}^{-1}$), the temperature difference of inlet and outlet feed streams (K), the total input energy (kWh) consumed by the circulating feed, and the total mass of distillate produced (m^3), respectively.

4. *Thermal efficiency*: Thermal efficiency η_{th} in MD is the ratio of energy of distillate to that of actual energy used [44]. It is also called first law efficiency. It can be expressed as:

$$\eta_{th} = \frac{Q_v}{Q_v + Q_c} \quad (31)$$

$$\eta_{th} = \frac{J * A_m * h_{fg}}{Q_{in}} \quad (32)$$

Where J , A_m , h_{fg} , Q_m , Q_v , and Q_c are distillate flux ($\text{kg}\cdot\text{m}^{-2}\text{h}^{-1}$), membrane active area (m), latent heat of vaporization ($\text{kJ}\cdot\text{kg}^{-1}\text{K}^{-1}$), heat flux through membrane ($\text{W}\cdot\text{m}^{-2}$), heat energy of vaporization ($\text{kJ}\cdot\text{kg}^{-1}\text{K}^{-1}$) and heat of condensation ($\text{kJ}\cdot\text{kg}^{-1}\text{K}^{-1}$), respectively. The Q_{in} can be expressed as shown in Eq. (29)

To improve the thermal efficiency, the heat conduction Q_c should be minimized by using higher thickness membranes, an air gap etc. However, this may require optimizing other parameters as well. Thermal efficiency matches with the GOR if there is no heat recovery [43].

5. *Second law efficiency*: First law efficiency generally used to compare systems with same energy source. However, if the energy source is different, the two systems can not be compared fairly. Using second law efficiency, exergies are compared instead. Therefore, systems can be compared regardless of their energy source. Exergy is the maximum available work extracted from the system when the system moves from its initial state to equilibrium.

Figure 12 shows a representation of second law efficiency. The first law expression can be deduced as [47]:

$$\dot{Q}_H + (\dot{m} \cdot h)_{sw} = \dot{Q}_0 + (\dot{m} \cdot h)_d + (\dot{m} \cdot h)_{br} \quad (33)$$

$$\dot{Q}_H - \dot{Q}_0 = (\dot{m} \cdot h)_d + (\dot{m} \cdot h)_{br} - (\dot{m} \cdot h)_{sw} \quad (34)$$

The second law can be expressed as:

$$\frac{\dot{Q}_H}{T_0} - \frac{\dot{Q}_0}{T_0} = (\dot{m} \cdot s)_d + (\dot{m} \cdot s)_{br} - (\dot{m} \cdot s)_{sw} + \dot{s}_{gen} \quad (35)$$

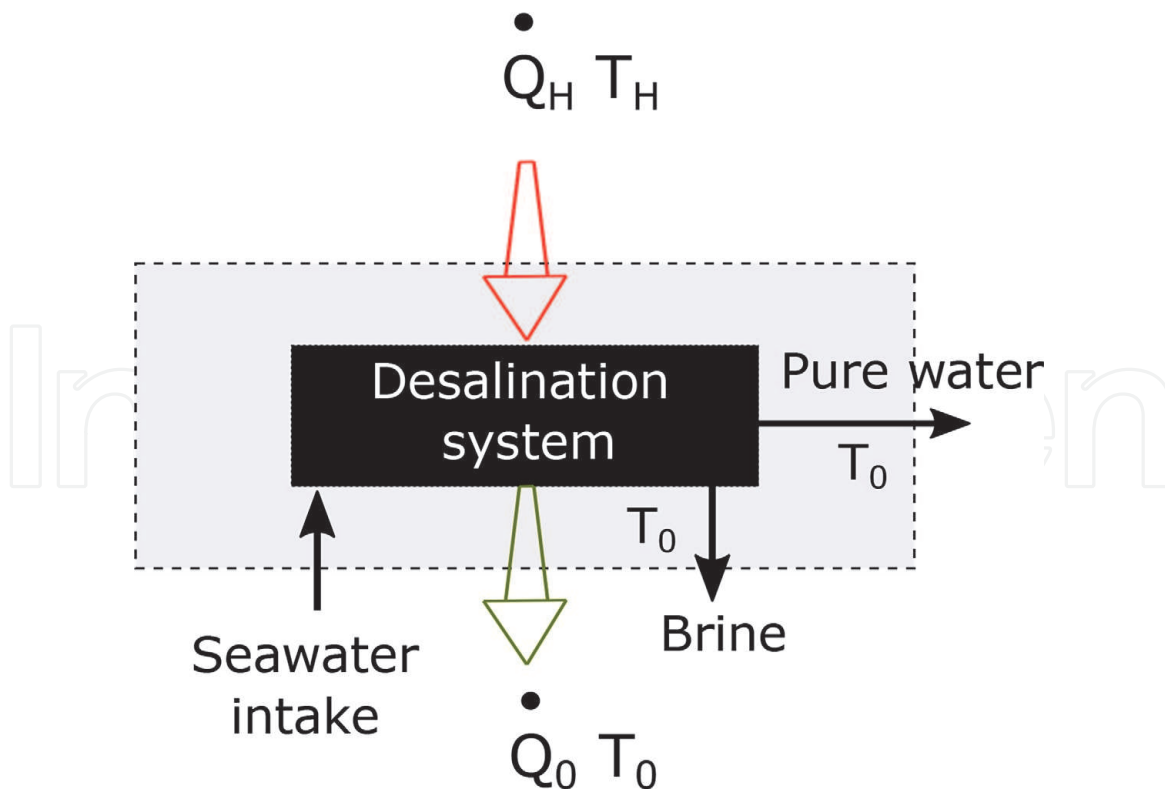


Figure 12.
 A schematic diagram of a black-box desalination system with heat transfer occurring from an external heat source at temperature T_H , and to the environment at temperature T_0 .

Multiplying second law equation Eq. (35) by T_0 and subtracting from Eq. (34):

$$\left(1 - \frac{T_0}{T_H}\right) \frac{\dot{Q}_H}{\dot{m}_d} = (G_d - G_{br}) - \frac{1}{RR} (G_{sw} - G_{br}) + T_0 \frac{\dot{S}_{gen}}{\dot{m}_d} = \frac{\dot{W}_{sep}}{\dot{m}_d} \quad (36)$$

Where RR is the recovery ratio $\frac{\dot{m}_p}{\dot{m}_{sw}}$, G is the Gibbs free energy ($h - T.s$). The second law efficiency can be expressed as:

$$\eta_{II} = \frac{\dot{W}_{separation}}{\dot{W}_{used}} \quad (37)$$

6. Recovery ratio: Recovery rate (RR) is the distillate production relative to the input feed stream flow in the MD system [48]. It is expressed as:

$$RR = \frac{\dot{m}_d}{\dot{m}_f} * 100\% \quad (38)$$

A high recovery means a high distillate flow rate is obtained by a given feed flow. In a single pass MD system, feed recovery is very low as compared to other membrane systems. It is reported that the maximum recovery attained in single pass MD reached 10% even if 100% thermal efficiency is attained [49].

In the latest developments, hybridization of MD with existing technologies is used to improve the energy efficiency of MD. The MD has been successfully integrated with other processes as hybrid such as RO, MED, and FO. MD unit has been

successfully realized to treat RO brine and FO draw solution which is a challenging part of the process. A comprehensive review of different hybrid technologies with the MD is described by Ghaffour et al. [50]. Additionally, in-situ heating of the feed water inside the MD module, so-called localized heating, has been introduced recently. Localized heating has shown a decreased TP effect which ensures the delivery of heat energy at the site of the feed-membrane interface. It eliminates the circulation heat loss associated with the conventional bulk heating [17, 51].

Photothermal energy source is the prime consideration due to its renewable and ever-existing energy source where the heat is delivered directly to the MD membrane. Politano et al. introduced the photothermal concept in MD first time using surface plasmon effect of silver nanoparticles [52, 53]. Various organic, inorganic, and polymeric materials have also been investigated as photothermal materials in the MD system [6, 54–56].

Similarly, Joule heating elements and spacers have been used to deliver localized heating to the feed channel [57, 58]. Ahmed et al [17] recently demonstrated the TP reduction by using the electrothermal property of carbon nanostructure. They obtained a decrease of SEC by 58%. Hence, localized heating provides a relatively simple infrastructure for small-scale clean water generation in remote off-grid regions.

5. Conclusions

Membrane distillation (MD) is a promising technology for the separation and purification industry. It is a specific distillation process in which vapor molecules travel through a hydrophobic membrane. MD has several advantages, including low-grade heat input, less fouling propensity, ability to treat high saline water. Four typical membrane configurations, membrane characteristics, membrane modules, heat and mass transfer mechanisms, thermal efficiency, and operating parameters have been presented. The most important limitation that has to be considered with membrane distillation is temperature polarization, which reduces the trans-membrane temperature difference, hence the performance. MD is found to be most suitable when the input energy source is solar or waste heat, due to energy intensive nature of distillation process. The recent development in membrane technology allows MD to run in compact modular configurations such as spiral module configurations. The performance of MD is expressed in terms of flux output and the specific energy. Although flux is an important but not the only factor to demonstrate the performance of an MD system, energy input also plays an important role. The recent advances in localized heating make the MD more promising to operate on a bigger scale.

Acknowledgements

The authors would like to acknowledge King Abdullah University of Science and Technology (KAUST) for supporting the authors in preparing this manuscript.

Conflict of interest

The authors declare no competing financial interests.

Nomenclature

AGMD	Air gap membrane distillation
CAPEX	Capital expenditure
DCMD	Direct contact membrane distillation
EE	Energy efficiency
FS	Flat sheet
GOR	Gain output ratio
MD	Membrane distillation
OPEX	Operational expenditure
RO	Reverse osmosis
RR	Recovery ratio
SEC	Specific energy consumption
SEM	Scanning electron microscope
SGMD	Sweeping gas membrane distillation
TP	Temperature polarization
TDS	Total dissolved solids
TPC	Temperature polarization coefficient
VMD	Vacuum membrane distillation

Symbols

A_m	membrane surface area (m^2)
C	concentration ($\text{mol}\cdot\text{L}^{-1}$)
C_m	membrane mass transfer coefficient ($\text{kg}\cdot\text{m}^{-2}\cdot\text{s}^{-1}\cdot\text{Pa}^{-1}$)
c_p	specific heat capacity ($\text{J}\cdot\text{kg}^{-1}\cdot\text{K}^{-1}$)
α	water activity (—)
χ	membrane tortuosity (—)
δ	membrane thickness (M)
\dot{m}	mass flow rate ($\text{kg}\cdot\text{s}^{-1}$)
\dot{Q}	heat transfer rate (W)
η	efficiency (—)
γ	activity coefficient (—)
λ	molecular mean free path (m)
μ	viscosity ($\text{Pa}\cdot\text{s}$)
π	osmotic pressure (Pa)
Π	pi (3.14) (—)
ρ	density ($\text{kg}\cdot\text{m}^{-3}$)
σ	molecular collision diameter (m)
Θ	temperature polarization (—)
ε	membrane porosity (—)
D_p	diameter of pore (m)
D_w	diffusion coefficient of water ($\text{m}^2\cdot\text{s}^{-1}$)
G	Gibbs free energy ($\text{kJ}\cdot\text{kg}^{-1}$)
h	heat transfer coefficient ($\text{W}\cdot\text{m}^{-2}\cdot\text{K}^{-1}$)
h_{fg}	latent heat of vaporization ($\text{kJ}\cdot\text{kg}^{-1}$)
J	vapor flux ($\text{kg}\cdot\text{m}^{-2}\cdot\text{h}^{-1}$)
k_B	Boltzmann constant ($\text{J}\cdot\text{K}^{-1}$)
k_m	thermal conductivity ($\text{W}\cdot\text{m}^{-1}\cdot\text{K}^{-1}$)
K_n	Knudsen number (—)
M	molecular weight ($\text{kg}\cdot\text{mol}^{-1}$)

\dot{m}	mass flow rate ($\text{mg}\cdot\text{s}^{-1}$)
N_A	Avagadro's number (6.023×10^{23}) (mol^{-1})
Nu	Nusselt number (—)
p	partial pressure (Pa)
P	total pressure (Pa)
Pr	Prandtl number (—)
q	heat flux ($\text{W}\cdot\text{m}^2$)
\dot{Q}	heat transfer rate (kW)
r	pore radius (m)
R	universal gas constant ($\text{J}\cdot\text{mol}^{-1}\text{K}^{-1}$)
Sc	Schmidt number (—)
s	specific entropy generation ($\text{kJ}\cdot\text{kg}^{-1}\text{K}^{-1}$)
T	temperature (K)
t	time (s)
U	overall heat transfer coefficient ($\text{W}\cdot\text{m}^{-2}\cdot\text{K}^{-1}$)
v	specific volume ($\text{m}^3\cdot\text{kg}^{-1}$)
W	work (kW)
X	mole fraction (—)

Subscripts

0	natural state (—)
12	between input and output (—)
av	average (—)
b	bulk (—)
br	brine (—)
c	conduction (—)
d	distillate (—)
f	feed (—)
fb	bulk feed (—)
fg	fluid-gas (—)
g	gaseous state (—)
gen	generation (—)
H	heat (—)
m	membrane (—)
p	permeate (—)
pb	bulk permeate (—)
sw	seawater (—)
sat	saturation (—)
v	vapor (—)

IntechOpen


Author details

Mustakeem Mustakeem*, Sofiane Soukane, Muhammad Saqib Nawaz
and Noredine Ghaffour

Biological and Environmental Science and Engineering (BESE) Division, Water
Desalination and Reuse Center (WDRC), King Abdullah University of Science and
Technology (KAUST), Thuwal, Saudi Arabia

*Address all correspondence to: mustakeem.mustakeem@kaust.edu.sa

IntechOpen

© 2022 The Author(s). Licensee IntechOpen. This chapter is distributed under the terms
of the Creative Commons Attribution License ([http://creativecommons.org/licenses/
by/3.0](http://creativecommons.org/licenses/by/3.0)), which permits unrestricted use, distribution, and reproduction in any medium,
provided the original work is properly cited. 

References

- [1] Lawson KW, Lloyd DR. Membrane distillation. *Journal of Membrane Science*. 1997;**124**(1):1-25
- [2] Johnson RA, Nguyen MH. *Understanding Membrane Distillation and Osmotic Distillation*. New York: John Wiley & Sons; 2017
- [3] Burgoyne A, Vahdati M. Direct contact membrane distillation. *Separation Science and Technology*. 2000;**35**(8):1257-1284
- [4] Belessiotis V, Kalogirou S, Delyannis E. Chapter four—membrane distillation. *Thermal Solar Desalination: Methods and Systems*. 2016;**201**:191-251
- [5] Alkhudhiri A, Hilal N. Membrane distillation—Principles, applications, configurations, design, and implementation. In: *Emerging Technologies for Sustainable Desalination Handbook*. Amsterdam, Netherlands: Elsevier; 2018. pp. 55-106
- [6] Zhani K, Zarzoum K, Ben Bacha H, Koschikowski J, Pfeifle D. Autonomous solar powered membrane distillation systems: State of the art. *Desalination and Water Treatment*. 2016;**57**(48–49): 23038-23051
- [7] Alkhudhiri A, Darwish N, Hilal N. Membrane distillation: A comprehensive review. *Desalination*. 2012;**287**:2-18
- [8] Kebria MRS, Rahimpour A. *Membrane Distillation: Basics, Advances, and Applications*. Rijeka: IntechOpen; 2020
- [9] Narayan A, Pitchumani R. Analysis of an air-cooled air gap membrane distillation module. *Desalination*. 2020; **475**:114179
- [10] Al-Zoubi H, Al-Amri F, Khalifa AE, Al-Zoubi A, Muhammad A, Ebtehal Y, et al. A comprehensive review of air gap membrane distillation process. *Desalination and Water Treatment*. 2018;**110**:27-64
- [11] Khayet M, Matsuura T. Chapter 11—Sweeping Gas Membrane Distillation. *Membrane Distillation: Principles and Applications*. Amsterdam, The Netherlands: Elsevier; 2011
- [12] Suárez F, Tyler SW, Childress AE. A theoretical study of a direct contact membrane distillation system coupled to a salt-gradient solar pond for terminal lakes reclamation. *Water Research*. 2010;**44**(15):4601-4615
- [13] Gryta M, Tomaszewska M, Morawski A. Membrane distillation with laminar flow. *Separation and Purification Technology*. 1997;**11**(2): 93-101
- [14] Drioli E, Ali A, Macedonio F. Membrane distillation: Recent developments and perspectives. *Desalination*. 2015;**356**:56-84
- [15] Khayet M, Matsuura T. Chapter 10—Direct Contact Membrane Distillation. *Membrane Distillation: Principles and Applications*. Amsterdam, The Netherlands: Elsevier; 2011
- [16] Thomas N, Mavukkandy MO, Loutatidou S, Arafat HA. Membrane distillation research & implementation: Lessons from the past five decades. *Separation and Purification Technology*. 2017;**189**:108-127
- [17] Ahmed FE, Lalia BS, Hashaikeh R, Hilal N. Alternative heating techniques in membrane distillation: A review. *Desalination*. 2020;**496**:1-14
- [18] Al-Obaidani S, Curcio E, Macedonio F, Di Profio G, Al-Hinai H, Drioli E. Potential of membrane

- distillation in seawater desalination: thermal efficiency, sensitivity study and cost estimation. *Journal of Membrane Science*. 2008;**323**(1):85-98
- [19] Olatunji SO, Camacho LM. Heat and mass transport in modeling membrane distillation configurations: A review. *Frontiers in Energy Research*. 2018;**6**:130
- [20] Summers EK, Arafat HA, Lienhard JH. Energy efficiency comparison of single-stage membrane distillation (md) desalination cycles in different configurations. *Desalination*. 2012;**290**:54-66
- [21] Anvari A. Mitigation of Temperature Polarization and Mineral Scaling in Membrane Distillation: The Impact of Induction Heated Elements. PhD thesis, Temple University; 2020
- [22] Camacho LM, Dumée L, Zhang J, Li J-d, Duke M, Gomez J, et al. Advances in membrane distillation for water desalination and purification applications. *Water*. 2013;**5**(1):94-196
- [23] Schofield R, Fane A, Fell C. Heat and mass transfer in membrane distillation. *Journal of Membrane Science*. 1987;**33**(3):299-313
- [24] Rizvi SS, Pabby AK, Sastre AM. *Handbook of Membrane Separations: Chemical, Pharmaceutical, Food, and Biotechnological Applications*. London: CRC Press; 2009
- [25] L. Martinez-Diez, M. Vázquez-González, and F. Florido-Diaz, Temperature Polarization Coefficients in Membrane Distillation. Taylor & Francis; 1998
- [26] Alsaadi AS, Francis L, Amy GL, Ghaffour N. Experimental and theoretical analyses of temperature polarization effect in vacuum membrane distillation. *Journal of Membrane Science*. 2014;**471**: 138-148
- [27] Martinez D, Vazquez-Gonzalez M, Florido-Diaz F. Study of membrane distillation using channel spacers. *Journal of Membrane Science*. 1998;**144**: 45-56
- [28] Velazquez A, Mengual JI. Temperature polarization coefficients in membrane distillation. *Industrial & engineering chemistry research*. 1995; **34**(2):585-590
- [29] Kim Y-D, Thu K, Ghaffour N, Ng KC. Performance investigation of a solar-assisted direct contact membrane distillation system. *Journal of Membrane Science*. 2013;**427**:345-364
- [30] Curcio E, Drioli E. Membrane distillation and related operations—A review. *Separation & Purification Reviews*. 2005;**34**(1):35-86
- [31] Kim Y-D, Francis L, Lee J-G, Ham M-G, Ghaffour N. Effect of non-woven net spacer on a direct contact membrane distillation performance: Experimental and theoretical studies. *Journal of Membrane Science*. 2018;**564**:193-203
- [32] Seo J, Kim YM, Kim JH. Spacer optimization strategy for direct contact membrane distillation: Shapes, configurations, diameters, and numbers of spacer filaments. *Desalination*. 2017; **417**:9-18
- [33] Shakaib M, Hasani SMF, Ahmed I, Yunus RM. A CFD study on the effect of spacer orientation on temperature polarization in membrane distillation modules. *Desalination*. 2012;**284**: 332-340
- [34] Taamneh Y, Bataineh K. Improving the performance of direct contact membrane distillation utilizing spacer-filled channel. *Desalination*. 2017;**408**: 25-35

- [35] Chen X, Vanangamudi A, Wang J, Jegatheesan J, Mishra V, Sharma R, et al. Direct contact membrane distillation for effective concentration of perfluoroalkyl substances: Impact of surface fouling and material stability. *Water Research*. 2020;**182**:116010
- [36] Alklaibi AM, Lior N. Membrane-distillation desalination: Status and potential. *Desalination*. 2005;**171**(2): 111-131
- [37] Martinez L, Rodriguez-Maroto JM. On transport resistances in direct contact membrane distillation. *Journal of Membrane Science*. 2007;**295**(1-2): 28-39
- [38] Martinez-Diez L, Florido-Diaz F. Desalination of brines by membrane distillation. *Desalination*. 2001;**137**(1-3): 267-273
- [39] Khayet M, Matsuura T. Chapter 10—Direct Contact Membrane Distillation. Amsterdam, Netherlands: Elsevier; 2011. pp. 249-293
- [40] Lee J-G, Alsaadi AS, Karam AM, Francis L, Soukane S, Ghaffour N. Total water production capacity inversion phenomenon in multi-stage direct contact membrane distillation: A theoretical study. *Journal of Membrane Science*. 2017;**544**:126-134
- [41] Ali A, Criscuoli A, Macedonio F, Drioli E. A comparative analysis of flat sheet and capillary membranes for membrane distillation applications. *Desalination*. 2019;**456**:1-12
- [42] Winter D, Koschikowski J, Wiegand M. Desalination using membrane distillation: Experimental studies on full scale spiral wound modules. *Journal of Membrane Science*. 2011;**375**(1-2):104-112
- [43] Warsinger DM, Nejati S, Juybari HF. Energy efficiency metrics in membrane distillation. In: *Advances in Water Desalination Technologies*. Singapore: World Scientific; 2021. pp. 263-288
- [44] Khayet M. Solar desalination by membrane distillation: Dispersion in energy consumption analysis and water production costs (a review). *Desalination*. 2013;**308**:89-101
- [45] Qtaishat MR, Banat F. Desalination by solar powered membrane distillation systems. *Desalination*. 2013;**308**:186-197
- [46] Jantaporn W, Ali A, Aimar P. Specific energy requirement of direct contact membrane distillation. *Chemical Engineering Research and Design*. 2017; **128**:15-26
- [47] Warsinger DEM. Thermodynamic Design and Fouling of Membrane Distillation Systems. PhD thesis, Massachusetts Institute of Technology; 2015
- [48] Saffarini RB, Summers EK, Arafat HA, et al. Technical evaluation of stand-alone solar powered membrane distillation systems. *Desalination*. 2012; **286**:332-341
- [49] Lokare OR, Tavakkoli S, Khanna V, Vidic RD. Importance of feed recirculation for the overall energy consumption in membrane distillation systems. *Desalination*. 2018;**428**:250-254
- [50] Ghaffour N, Soukane S, Lee J-G, Kim Y, Alpatova A. Membrane distillation hybrids for water production and energy efficiency enhancement: A critical review. *Applied Energy*. 2019; **254**:113698
- [51] Wu X, Jiang Q, Ghim D, Singamaneni S, Jun Y-S. Localized heating with a photothermal polydopamine coating facilitates a novel membrane distillation process. *Journal of Materials Chemistry A*. 2018;**6**(39): 18799-18807

[52] Politano A, Di Profio G, Fontananova E, Sanna V, Cupolillo A, Curcio E. Overcoming temperature polarization in membrane distillation by thermoplasmonic effects activated by ag nanofillers in polymeric membranes. *Desalination*. 2019;**451**:192-199

[53] Politano A, Argurio P, Di Profio G, Sanna V, Cupolillo A, Chakraborty S, et al. Photothermal membrane distillation for seawater desalination. *Advance Material*. 2017;**29**(2):1-6

[54] Razaqpur AG, Wang Y, Liao X, Liao Y, Wang R. Progress of photothermal membrane distillation for decentralized desalination: A review. *Water Research*. 2021;**201**:117299

[55] Huang L, Pei J, Jiang H, Hu X. Water desalination under one sun using graphene-based material modified PTFE membrane. *Desalination*. 2018;**442**:1-7

[56] Ghim D, Wu X, Suazo M, Jun Y-S. Achieving maximum recovery of latent heat in photothermally driven multi-layer stacked membrane distillation. *Nano Energy*. 2021;**80**:1-10

[57] Mustakeem M, Qamar A, Alpatova A, Ghaffour N. Dead-end membrane distillation with localized interfacial heating for sustainable and energy-efficient desalination. *Water Research*. 2021;**189**:116584

[58] Tan YZ, Ang EH, Chew JW. Metallic spacers to enhance membrane distillation. *Journal of Membrane Science*. 2019;**572**:171-183